236U analyses with the ETH Zurich MILEA prototype system

Journal Article

Author(s):
Christl, Marcus; Gautschi, Philip; Maxeiner, Sascha; Müller, Arnold Milenko; Vockenhuber, Christof; Synal, Hans-Arno

Publication date:
2023-01-01

Permanent link:
https://doi.org/https://doi.org/10.3929/ethz-b-000584180

Originally published in:
Nuclear Instruments and Methods in Physics Research Section B: Beam Interactions with Materials and Atoms 534, https://doi.org/10.1016/j.nimb.2022.11.009

Funding acknowledgement:
- New Developments in Ion Beam Physics ()

Nuclear Instruments and Methods in Physics Research B 534 (2023) 61–71

Contents lists available at ScienceDirect

Nuclear Inst. and Methods in Physics Research, B

journal homepage: www.elsevier.com/locate/nimb

^{236}U analyses with the ETH Zurich MILEA prototype system

Marcus Christl [a,*], Philip Gautschi [a], Sascha Maxeiner [b,a], Arnold Milenko Müller [a,b], Christof Vockenhuber [a], Hans-Arno Synal [a]

[a] Laboratory of Ion Beam Physics, ETH Zurich, 8093 Zurich, Switzerland
[b] Ionplus AG, Lerzenstrasse 12, 8953 Dietikon, Switzerland

ARTICLE INFO

Keywords:
Accelerator Mass Spectrometry
Actinides
Compact AMS
MILEA
U-236
Puisotopes

ABSTRACT

Compact, low energy accelerator mass spectrometry (AMS) has evolved over the past years as one of the most sensitive, selective, and robust techniques for the analysis of heavy and long lived radionuclides. In this study, we focus on the analytical capabilities of the compact AMS system MILEA, mainly for ^{236}U analyses. First, the setup of the system for actinide analyses is presented and the special technical setup for $^{23x}U/^{238}U$ (x = 3, 6, 5) is discussed. Then, the background and sensitivity for $^{236}U/^{238}U$ are studied in detail, and finally results from the first routine runs are presented and discussed. Our results show that the ETH Zurich MILEA system is ideally suited for fast, reliable, high sensitivity, and almost background free analyses of $^{236}U/^{238}U$ in environmental samples allowing the analysis of larger batches of samples with reasonably small sample sizes or volumes.

1. Introduction

Over the past decade the long lived anthropogenic U-isotopes ^{236}U ($T_{½}$ = 23.4 Myr) and ^{233}U ($T_{½}$ = 159 kyr) evolved as new and powerful anthropogenic tracers in oceanographic studies or for source apportionment of contaminated materials [1–6]. This success was supported by substantial developments in accelerator mass spectrometry (AMS) that allow the fast, precise, and almost background free determination of anthropogenic Pu- and U-isotopes in environmental samples [7–10]. The success of compact, low energy AMS systems in actinide research is not limited to the major actinides alone, it also triggered several studies relying on the highly sensitive and selective detection of the minor actinides (e.g. Np-, Am-, *Cm*-isotopes) in environmental and biological samples [11–17].

Compact, low energy AMS is used for the detection of actinides since the 2000s [18–20]. Although those systems were not optimized for actinide measurements initial results indicated that they can compete with the performance of much bigger and more complex AMS systems [19]. In the following years several technical advances resulted in the breakthrough of compact AMS systems not only for the detection of heavy ions [21–23]. Milestones in that process represent advances in particle detection [24,25], the implementation of He-stripping [8,26], and the development of dedicated simulation tools for low energy AMS systems [27,28]. Combining the above improvements and tools resulted in the development of a prototype multi isotope AMS system at ETH Zurich that is optimized for the efficient and low background detection of light (^{10}Be, ^{14}C, ^{26}Al) and heavy (^{129}I, actinides) ions [29].

Here we report on the setup and the performance of the MILEA prototype AMS system installed at the Laboratory of Ion Beam Physics of ETH Zurich for the analysis of U- and to a minor extent also Pu-isotopes. We demonstrate that the ETH Zurich MILEA system is ready for state-of-the-art analyses of ultra-trace levels of actinides in environmental samples.

2. Material and methods

2.1. The ETH Zurich MILEA system

The 300 kV **M**ulti-**I**sotope **L**ow **E**nergy **A**MS system MILEA is a joint development of Ionplus AG and ETH Zurich. Measurements for this study were performed with the prototype system built and installed in 2018/2019 at the Laboratory of Ion Beam Physics, ETH Zurich. The system is optimized for the measurement of ^{14}C, ^{10}Be, ^{26}Al, ^{41}Ca, ^{129}I, and actinides at low energies [30].

The low energy (LE) side of the MILEA system consists of a multi cathode MICADAS-type Cs-sputtering negative ion source [21], operating at voltages of up to 50 kV, and a combination of a 90° electrostatic analyzer (LE-ESA, r = 534 mm) and a 90° magnet (LE-magnet, r = 450 mm) that allows achromatic injection of the negative ion beam into the accelerator and stripper. The LE-magnet is equipped with a fast

* Corresponding author.
E-mail address: mchristl@phys.ethz.ch (M. Christl).

https://doi.org/10.1016/j.nimb.2022.11.009
Received 15 December 2021; Received in revised form 2 November 2022; Accepted 5 November 2022
Available online 24 November 2022
0168-583X/

bouncing system that enables fast, sequential injection of different masses into the accelerator. Two movable Faraday cups on the LE-side positioned on each side of the beam axis in front of the accelerator allow monitoring of the negative ion current and the determination of ion beam transmission through the accelerator.

The accelerator consists of a vacuum insulated high voltage platform, which can be operated at maximum acceleration voltages of 300 kV provided by a solid-state high voltage power supply from Heinzinger GmbH. The high voltage terminal contains the stripper tube, where He gas that is fed from ground potential is used to transform the incident negative ion beam into positive ions and to disintegrate molecular isobars. The following electrostatic quadrupole triplet lens allows optimal focusing of different charge states and molecular break-up products so that the isotope of interest matches with the ion optical conditions of the high energy (HE) spectrometer [30].

The HE spectrometer consists of two momentum (p/q) filters (90° HE1 magnet, r = 600 mm and 110° HE2 magnet, r = 600 mm) and an energy (E/q) filter (120° ESA, r = 620 mm) placed between them. Seven moveable Faraday Cups (HE FC) that are placed in the analysis chamber after the HE1 magnet allow to measure the ion currents of stable or abundant nuclides for the various AMS setups. HE FC 1 – 4 located on the right hand side of the rare isotope beam axis are used for the stable nuclide(s) detection during ^{14}C, ^{10}Be, ^{41}Ca, ^{129}I measurements and FC 5 – 7 are placed on the left hand side for U-isotopes and ^{26}Al measurements. Taking into account the spatial separation of different isotopes two versions of FCs have been designed with an opening width of 14 mm (HE FC 1,2,3 & 7) and 8 mm (HE FC 4, 5 & 6), with the smaller FCs used for ^{127}I, ^{238}U and ^{235}U current measurements.

Detection of rare nuclides is performed by an ETH Zurich designed two-anode gas ionization chamber (GIC) [25] that additionally can be equipped with a gas absorber cell [31]. Six apertures can be set at the focal points of the system (A1 – A6 in Fig. 1).

2.2. Ion source modification and targets used

During the first two years of operation the ion source was significantly modified from the initial setup. A new extractor was installed and the polarity of the extraction lens was changed to positive voltage. Furthermore, a Cs nozzle with higher conductance was installed that allows a significantly higher Cs flux onto the sample (this research was conducted as part of Horizon 2020 research and innovation program, grant agreement No 824096, WP20, JRA1, Ion Sources and Beams, publication in progress). With these modifications, we were able to extract much higher negative currents of BeO and UO compared to the previous setup and we observed higher over-all efficiencies. Since the results presented here have been obtained with both ion source setups, we indicate with which setup the data has been collected when this becomes relevant.

The ion source of the MILEA system is designed to accept standard MICADAS type targets [21]. However, to gain flexibility and the ability to switch AMS analyses between the two multi isotope systems at ETH Zurich (Tandy and MILEA) we decided to continue with using the modified NEC cathode holders that are routinely used at the Tandy system [32]. Therefore, an adapter was designed that allows to measure samples pressed in Tandy cathodes on MILEA [33]. All results presented here are based on oxide matrices and the extraction of a negative actinide oxide beam as routinely applied at ETH Zurich for actinide analyses [7].

2.3. Setup for actinide measurements

All measurements presented here were performed with the compact 300 kV AMS system MILEA built and installed at ETH Zurich as described above. For actinide measurements a terminal voltage of around 260 kV is applied, which is limited by the bending capability of the HE-magnets. Taking into account the sum of ion source and sample potential of 46 kV and the molecular breakup from the oxide injection, the stripping energy of actinide ions is about 285 keV. Selecting the three plus charge state the final actinide ion energy is slightly above 1 MeV. For detection of the rare actinide isotopes the signal from the first anode of the GIC is used. A 3 × 3 mm^2 or a 4 × 4 mm^2 SiN detector entrance window of 30 nm thickness is used for actinide analyses.

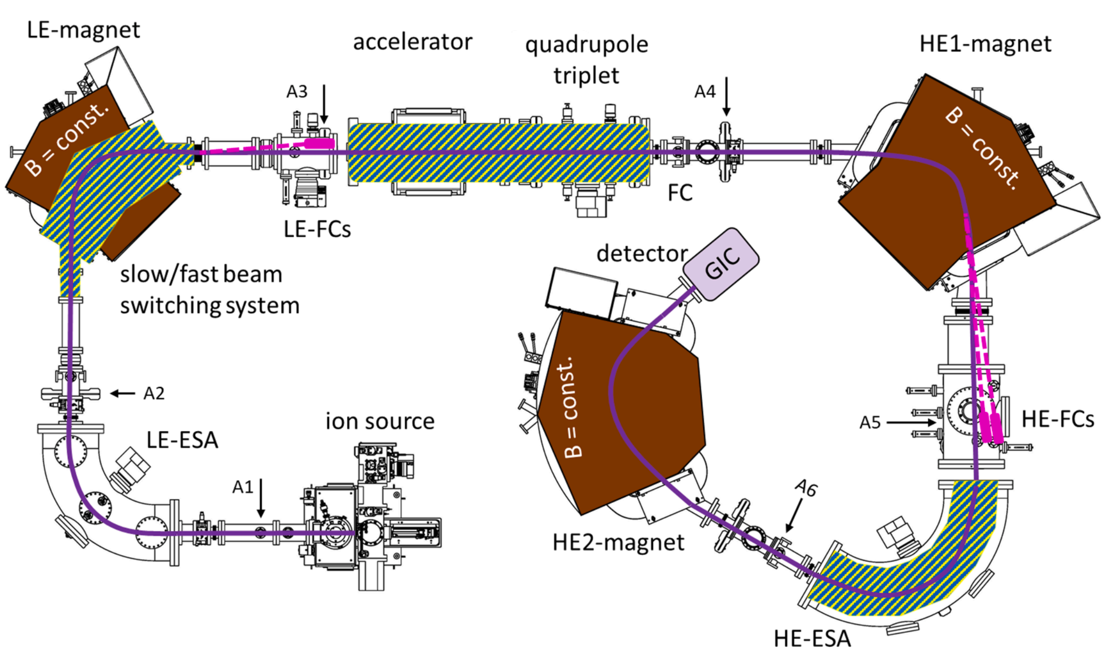

Fig. 1. Actinide setup MILEA. Setup of the ETH Zurich MILEA system for actinide measurements. All magnets are kept at constant B-field (brown), while the injection of different radionuclides into the detector is achieved by adjusting four electrostatic devices: the bouncing system, the accelerator voltage, the quadrupole triplet lens, and the ESA (blue/yellow hatched devices). A1-6 mark the position of apertures that can be inserted into the central beam line. The positions of the off-axis Faraday Cups for U-isotope measurements are indicated in magenta. (For interpretation of the references to colour in this figure legend, the reader is referred to the web version of this article.)

2.3.1. Setup for Pu and the higher actinides

Due to the low abundance of Pu-isotopes or isotopes of the higher actinides, FCs cannot be used for detection. The determination of isotopic ratios of the rare actinides is done by sequential injection of each isotope into the GIC. To enable reproducible sequential switching between different rare isotopes all three magnets (p/q filters) are kept at constant field (brown shaded devices in Fig. 1), which implies that different isotopes (masses) are analyzed at different energies. Thus, the accelerator and the HE-ESA have to be adjusted in a way that keeps the p/q ratio of the different isotopes constant.

The injection of the negative actinide oxide beam of interest is performed by applying a constant voltage to the chamber of the low energy magnet. Additionally, the electrostatic quadrupole triplet lens is adjusted to account for the different focusing of the selected masses from the molecular breakup of the actinide oxide injection (blue/yellow shaded devices in Fig. 1). Switching between rare isotopes takes less than one second. The above described method to switch between different rare actinide isotopes is used at several AMS systems worldwide and allows precise measurements of isotopic ratios of actinides [34–36]. It is generally referred to as slow sequential switching or cycling.

2.3.2. Setup for $^{x}U/^{238}U$ measurements (x = 233, 236, 235)

The standard setup for ^{236}U measurements at the ETH MILEA and Tandy systems consists of a combination of three slow sequential cycling sequences (as described above) with fast cycling of the abundant ^{238}U isotope (including $^{238}U^{16}O^{-}$). In the first slow cycling sequence ($^{233}U/^{238}U$, Fig. 2a) $^{233}U^{16}O$ is injected and the accelerator, quadrupole lens and HE-ESA are set so that $^{233}U^{3+}$ reaches the GIC (yellow shaded devices in Fig. 2a). The duration of the first slow sequence is typically 5–60 s depending on the expected counting rate of ^{233}U (e.g. spiked vs natural signal). During this sequence the fast bouncing system is used to measure the negative $^{238}U^{16}O$ current and the $^{238}U^{3+}$ current in the LE- and HE-FC6, respectively. In the second slow cycling sequence ($^{236}U/^{238}U$, Fig. 2b) $^{236}U^{16}O$ is injected and all electrostatic devices on the HE side are tuned to ^{236}U reaching the GIC (blue shaded devices in Fig. 2b). The duration of the second sequence is typically 30 s, depending on the expected ^{236}U counting rate. Also, during this sequence, the fast bouncing system is used to measure the $^{238}U^{16}O^{-}$ and the $^{238}U^{3+}$ currents on the LE and HE side (FC5 in Fig. 2b), respectively. In the third slow cycling sequence ($^{235}U/^{238}U$, Fig. 2c) $^{235}U^{16}O$ is injected but the accelerator and the quadrupole are set to ^{233}U settings (yellow labelled devices). As a consequence, $^{235}U^{3+}$ does not reach the GIC but can be analyzed in quasi DC mode in FC5 on the HE side. The duration of the third slow sequence is about 5 s. The fast bouncing system is still used to measure the $^{238}U^{16}O^{-}$ current on the LE side and the $^{238}U^{3+}$ current in FC6 on the HE side. Details of the cup configuration are displayed in the lower part of Fig. 2, details on the current measurement are discussed in section 2.4.1 below.

2.4. Machine parameter and sensitivity studies

To document the performance of the ETH Zurich MILEA system for the AMS analysis of $^{236}U/^{238}U$ (and Pu-isotopes) several experiments were conducted to study in detail the background and the sensitivity of the machine. The technical setup and the methods used to analyze the results are described in the following.

2.4.1. Current integrator

Each FC of the MILEA system is connected to an in house designed current integrator that enables precise determination of positive or negative ion currents in fast bouncing mode. The fast bouncing mode allows during all slow cycling sequences (described in section 2.3.2) the determination of $^{238}U^{16}O^{-}$ and $^{238}U^{3+}$ currents at a repetition rate of 12.5 Hz. The full range of each current integrator can be adjusted according to the expected sample currents. For a standard ^{236}U measurement the current integrators are typically set to the ultra-sensitive mode (here) providing 10nA full range. With this setting a single (fast bounced) current measurement takes less than 1 ms. Several single current measurements are averaged during one slow cycling sequence (i. e. while the rare nuclide is counted). The time over which the current measurements are averaged depends on the counting time for the rare

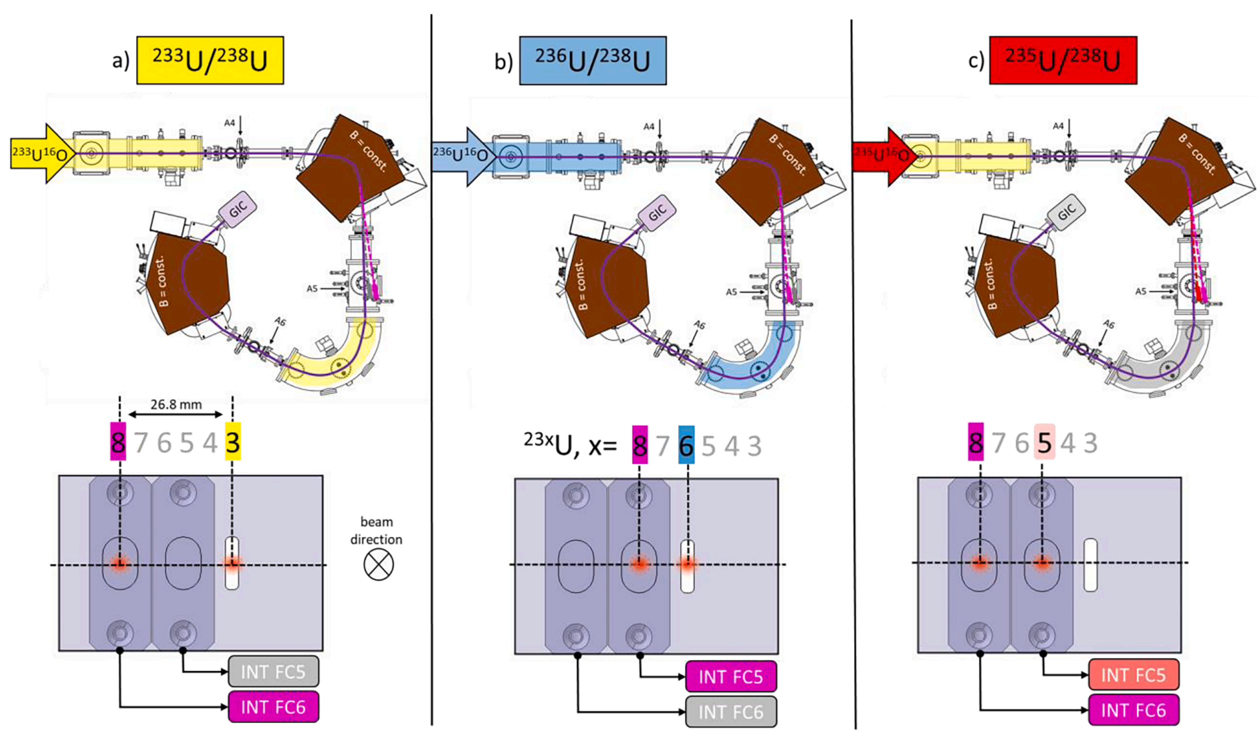

Fig. 2. Setup and cup configuration for u-isotopes: Standard setup for U-isotope measurements and cup configuration. a) Setup and cup configuration for $^{233}U/^{238}U$, b) setup and cup configuration for $^{236}U/^{238}U$, c) setup and cup configuration for $^{235}U/^{238}U$ (see main text for details).

nuclide (i.e. the length of the actual slow cycling sequence). If, for example, a counting time (slow cycling length) of 10 s is chosen for ^{236}U in the GIC, the according $^{238}U^{3+}$ and $^{238}U^{16}O^{-}$ current measurements are averaged over the same time period with 10 s × 12.5 Hz = 125 individual current determinations for one $^{236}U/^{238}U$ ratio and one transmission measurement. We note that the full range and repetition rate of the current integrators can be adjusted by software and thus can be adopted to special needs of the experiment.

The MILEA current integrators are designed and calibrated in a way that they produce a very small artificial current offset which is later subtracted by the machine's software. To document the linearity and to determine the offset of the current integrators we connected an external variable current source and recorded the integrator output after a sequence of 5 measurements with 3 s integration time (mean and standard deviation of the current measurements were calculated). The current of the external source was checked before and after each sequence using a Keithley picoampere meter.

2.4.2. *Charge state yields for ^{238}U*

Transmission measurements were performed for ^{238}U at three different stripping energies between 182 keV and 281 keV. To minimize beam losses a special, large diameter (25 mm) FC was used that was temporarily mounted in the HE-FC chamber (Fig. 1) for the duration of the experiment. No apertures were inserted to constrain the beam. For each chosen stripping energy, transmission was recorded for the 3+ and 4+ charge states while varying the He-stripper gas pressure (stripper scans). The accelerator voltage was adjusted with increasing stripper gas density to compensate for the increased energy losses. For the lowest energy (182 keV) also the 2+ charge state was analyzed, which was not possible for the higher energies due to the limited bending power of the HE1 magnet. The pressure in the accelerator tank was used as a proxy for the stripper gas density. The relation between tank pressure and stripper gas density was calibrated using the relative energy loss of carbon ions in He [37]. Charge state yields were determined by correcting the transmission measurements for scattering losses using SRIM simulations carried out at three selected stripper densities (3, 6, and 12 × 10^{16} at/cm^2) [8,38,39].

We note that we did not extrapolate the exponential decline of the transmission measurements to zero stripper pressure [8,40] to determine the charge state yields of U in He. At very low stripper gas densities almost no beam losses are expected because the maximum single scattering angle of U in He (16.3 mrad) is smaller than the acceptance of the MILEA stripper (22 mrad). As beam losses only become relevant at higher stripper gas densities the extrapolation of the fit to zero density would lead to an overestimation of the charge state yields.

2.4.3. *Abundance sensitivity and transmission measurements*

Since no completely ^{236}U-free U-blank material is available the machine background for $^{236}U/^{238}U$ cannot be determined directly. The Vienna KkU-standard material (VKkU) with a nominal $^{236}U/^{238}U$ ratio of (69.8 ± 3.2) × 10^{-12} [10] ranges among the materials with the lowest $^{236}U/^{238}U$ ratios available in significant amounts at ETH Zurich. It has therefore been used for all background scans and for the abundance sensitivity measurements described below. The VKkU material has undergone chemical purification and is assumed not to contain detectable amounts of ^{239}Pu [40].

An often-applied method for the estimation of the background for $^{236}U/^{238}U$ measurements involves the determination of the abundance sensitivity (AS). In our case the AS is determined by measuring the tailing of an intense ^{238}U beam extracted from a VKkU sample onto the next higher mass (amu = 239). Assuming that the VKkU material does not contain any ^{239}Pu the measured amu(239)/^{238}U ratio has to be caused by tailing, scattering, etc. of ^{238}U. In this context, the AS provides a proxy for the background caused by ^{235}U on mass 236. Sequential switching between the AS measurement (amu(239)/^{238}U ratio) and the standard $^{236}U/^{238}U$ setup (Fig. 2b) further allows determining the HE-transmission (i.e. by comparing the measured $^{236}U/^{238}U$ ratio of the VKkU sample with its nominal value) and thus to calculate the standard normalized AS given as follows (cps: counts per second):

$$AS_{norm} = \frac{cps(amu_{239})}{cps(^{238}U)} \cdot \frac{\left(^{236}U/^{238}U\right)_{VKkU,nominal}}{\left(^{236}U/^{238}U\right)_{VKkU,\ measured}} \tag{1}$$

The normalized AS and the $^{236}U/^{238}U$ ratio including transmission for ^{238}U were determined for different stripper densities and using different apertures (A3, A5, and A6 in Fig. 1). This allows studying i) the charge state yield of $^{238}U^{3+}$ at the given stripping energy, and ii) the influence of the apertures and stripper gas density on the background for ^{236}U.

The VKkU samples used for the AS and background measurements contained about 2 mg of U-oxide mixed with ca. 3 mg of Nb powder. These so called VKkU_hc (high current) samples gave $^{238}U^{3+}$ current outputs at the order of several hundred nA and thus allowed the determination of AS and background with good counting statistics (see section 3.2).

2.4.4. *U/Pu efficiency tests*

The total measurement efficiency of the MILEA system for Pu and U extracted from an oxide sample matrix was determined using a combination of two purified spike solutions containing ^{233}U and ^{242}Pu. Well known amounts of both nuclides (about 1 pg) were co-precipitated with different amounts of Fe (Fe-hydroxide co-precipitation), then transferred to oxide form at 650 °C and finally mixed with different amounts of Nb-powder and pressed into Al-sample holders (Table 1). Two sets of samples were prepared and analyzed under different ion source settings, before and after the modification of the ion source (see section 2.2). Therefore, Cs-temperatures of both runs are not directly comparable. Since the modifications allowed for higher Cs-densities on the sample the second set of samples most probably received a higher Cs-flux at the same Cs-reservoir temperature.

Using the setup for Pu-measurements (section 2.3.1) the efficiency test samples were analyzed by switching every 60 s between ^{233}U and ^{242}Pu (slow cycling). Both isotopes were identified and counted with the GIC (Fig. 1). The detection efficiency was calculated for each isotope as the ratio of identified counts in the GIC divided by the number of atoms added to the sample. The resulting number was corrected for any idle time during which the sample was sputtered but the isotope of interest was not counted (e.g. because the other isotope was counted or because of beam switching). The total apparent detection efficiency is given by EQ2 with X representing the isotope of interest (^{233}U or ^{242}Pu):

Table 1
Two efficiency tests series (run 1, run 2) for actinide samples containing about 1 pg of ^{233}U and ^{242}Pu respectively. Samples are prepared in an oxide matrix with different amounts of Fe for co-precipitation and mixed with various amounts of Nb-powder for final target preparation. A maximum detection efficiency of about 1 % is reached for both, U and Pu.

ETH-Label	U-233 (pg)	Pu-242 (pg)	Fe (mg)	Nb (mg)	max. det. eff. U	max. det. eff. Pu
Run 2 (June 2021)						
ZP1300	1.05	1.07	1.2	3	0.4 %	0.3 %
ZP1301	1.06	1.07	2.5	3	0.7 %	0.5 %
ZP1302	1.02	1.07	1.3	6	0.5 %	0.4 %
ZP1303	1.04	1.07	2.5	6	0.9 %	0.7 %
ZP1304	1.06	1.04	1.3	9	0.6 %	0.5 %
ZP1305	1.06	1.09	2.6	9	1.0 %	0.7 %
Run 1 (December 2020)						
Pu1	1.04	1.05	1.5	3	0.4 %	0.5 %
Pu2	1.04	1.05	3.0	6	0.9 %	1.0 %
Pu3	1.03	1.05	6.0	6	0.8 %	0.8 %

$$eff_{det}(X) = \frac{\sum counts(X)}{spikedatoms(X)} \bullet \frac{\sum sputtertime(target)}{\sum meas.time(X)} \quad (2)$$

The total ionization efficiency was calculated using EQ3 assuming 33 % transmission (LE to the HE side) and 85 % HE-transmission:

$$eff_{ion}(X) = eff_{det}(X) \frac{1}{tra(LE-HE)} \bullet \frac{1}{tra(HE)} = eff_{det}(X) \bullet 3.6 \quad (3)$$

3. Results and discussion

3.1. Current measurements

The newly designed high sensitivity MILEA current integrators allow the measurement of currents in the sub-nA range within less than a millisecond (i.e. in fast bouncing mode). As an example for the excellent quality of the current integrators we show a linearity measurement of current integrator #5 (Fig. 3) in high sensitivity mode. The results are shown after the subtraction of the intrinsic current offset of (3.19 ± 0.07) pA (see section 2.4.1 for details). The full range of 10nA represents well the expected sample current range as during first routine $^{236}U/^{238}U$ measurements 2L sea water samples (containing less than 6.5 µg of ^{238}U) revealed currents of up to 3nA.

The linearity was tested between >10nA and several hundred fA, with the latter representing the lower limit of our external current source. The reduced R^2 of a linear fit applied to all data points documents the excellent linearity of the current integrator (Fig. 3). The slope of (0.99885 ± 0.00003) is very close to but significantly different from one. This is, however, not an issue since all routine AMS measurements are carried out relative to standards, which are measured with the same current integrators so that the slope cancels out when applying standard normalization. A non-zero current offset, in contrast, can have a significant effect on the standard normalized results and thus has to be avoided. The results presented in Fig. 3 show that the correction of the intrinsic offset of the integrator is robust. The uncertainty of 0.06 pA for the intercept (offset) documents that even in fast bouncing mode current measurements in the fA range are possible with the high sensitivity MILEA current integrators.

The results presented here are representative for all MILEA current integrators operating at different full ranges. In routine operation they

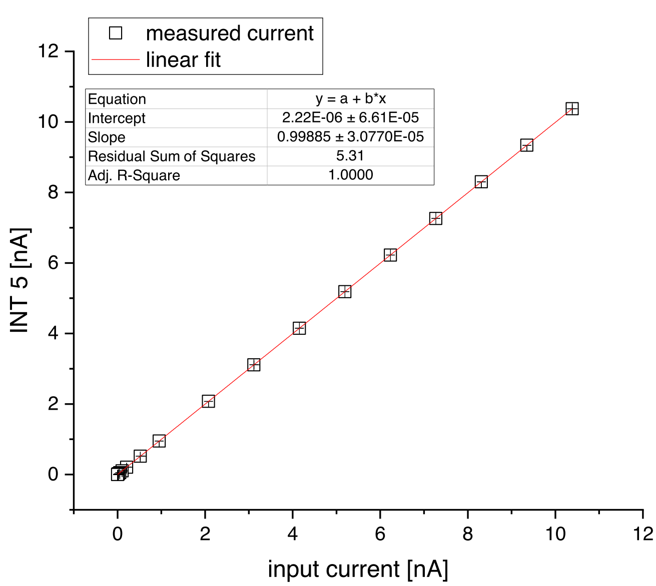

Fig. 3. MILEA current integrators. Example for the linearity and precision of the high sensitivity MILEA current integrators. The red line represents a linear fit to the measured data. (For interpretation of the references to colour in this figure legend, the reader is referred to the web version of this article.)

allow precise current measurements in fast bouncing mode at a repetition rate of 12.5 Hz and thus contribute to the reliable determination of isotopic ratios. In the context of ^{236}U measurements the high sensitivity MILEA current integrators indirectly enhance rare nuclide detection efficiency because only a small amount of measurement time has to be allocated for the current measurements. In the case we presented here (10 nA full range), only 3.5 % of the counting time is spent for LE and HE current measurements during the $^{236}U/^{238}U$ and $^{233}U/^{238}U$ sequences, respectively. With the routine setup for $^{236}U/^{238}U$ at the ETH Zurich Tandy system [7] almost 25 % of the measurement time had to be reserved for HE and LE current measurements due to the much lower sensitivity of the Tandy current integrators.

3.2. Transmission, sensitivity, and background

In this section we first present charge state yields of U in He at stripping energies of around 200 keV, then we discuss the transmission and background for routine analyses of ^{236}U, and finally we investigate the influence of the slit settings on the HE side on HE-transmission and AS.

3.2.1. Transmission and charge state yields for ^{238}U

Charge state yields were determined from stripper pressure scans (Fig. 4**a**) as described in section 2.4.2. As an example the stripper scans performed at 185 keV stripping energy are shown in Fig. 4**b** for all three charge states analyzed. An exponential fit was applied to the declining part of each transmission curve after having reached its maximum (dashed lines). Simulation based scattering corrections (section 2.4.2) applied at stripper densities of 3×10^{16} at/cm^2 and 6×10^{16} at/cm^2 yield consistent results for all investigated charge state yields (open circles in Fig. 4**b**) indicating that the experimentally determined relation between accelerator tank pressure gauge reading and stripper gas density is valid. For higher stripper gas densities (12×10^{16} at/cm^2) scattering corrections lead to systematically lower results for the charge state yields. At such high stripper gas densities additional losses e.g. due to energy straggling, the limited size of the FC,and simplified assumptions on the stripper geometry and the divergence of the incident ion beam become more important so that simplified scattering corrections are not sufficient anymore to calculate reliable charge state yields. The scattering corrections, for example, do not consider the divergence of the incident negative ion beam and the fact that a fraction of the incident beam might already be lost on the injection side of the stripper. These additional losses increase with stripper pressure and yield to an underestimation of the scattering corrected charge state yields at higher stripper pressures. From each stripper scan, we used the scattering corrected value at 3×10^{16} at/cm^2 as the final charge state yield (plotted in Fig. 4**a**, filled circles) because it is least influenced by model corrections.

We note that the calculated charge state yields are close to the maximum transmission values measured for the 3+ and 4+ charge states (Fig. 4**b**). This observation is consistent with the theory that predicts negligible scattering losses at low stripper densities where single scattering dominates. With 22 mrad the acceptance angle of the MILEA gas stripper is significantly larger than the maximum single scattering angle of U on He (16.3 mrad). As a consequence, the simple extrapolation of the exponential fits (dashed lines) to zero stripper pressure leads to an overestimation of the charge state yields.

A prominent overshooting of the 2+ charge state is observed at a stripping energy of 185 keV (Fig. 4**b**). Here, the transmission curve does not follow a simple exponential decrease after having reached maximum transmission. The observed maximum most probably represents a transient (non steady state) feature where the 2+ charge state is (over-) populated while 3+ and 4+ charge states evolve towards their respective equilibrium conditions. Evidence for this comes from the observation that the populations in the 3+ and 4+ charge states are still steeply rising with increasing stripper density when the 2+ exhibits its

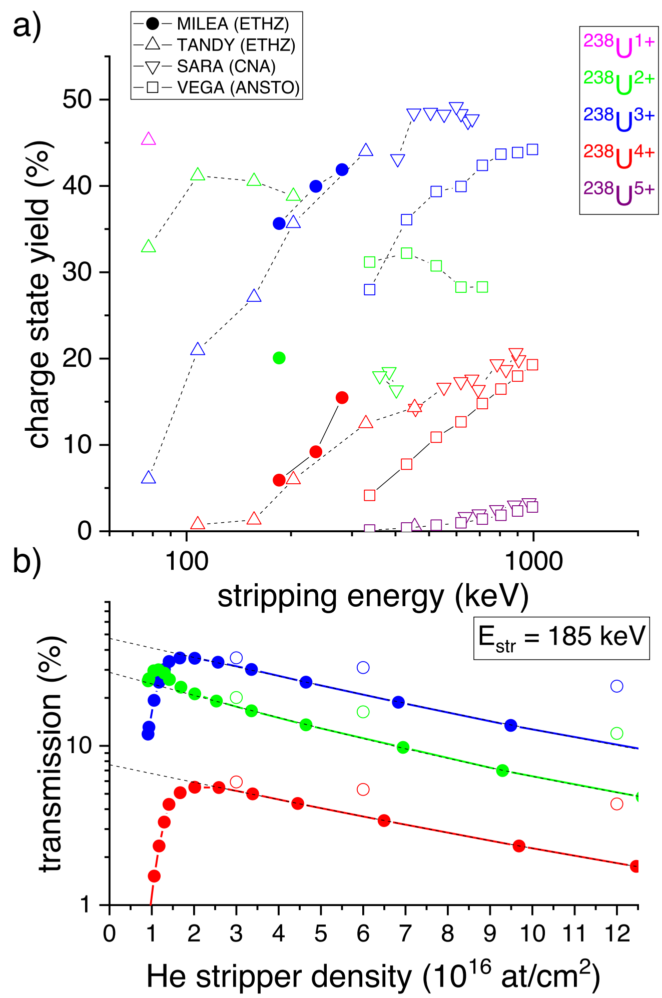

Fig. 4. Charge state yields and transmission. Transmission and charge state yields for U-ions in He. a) Charge state yields as a function of energy determined at different AMS systems. b) EXAMPLE for the determination of the charge state yields at MILEA at a stripping energy of 185 keV. Transmission was recorded as a function of energy for different charge states (filled circles). Data for stripper densities of 3, 6, and 12 × 10^{16} at/cm^2 were corrected for scattering losses using SRIM using the given acceptance angle of the MILEA stripper of 22 mrad (open circles). The dashed lines represent exponential fits to the declining part of the transmission curve.

(transient) maximum. In this special case, both, the extrapolation of the exponential fit to zero and the maximum transmission value would have led to a significant overestimation of the 2+ equilibrium charge state yield.

Routine analysis of $^{236}U/^{238}U$ is performed at a terminal voltage of 260 kV, which is equivalent to a stripping energy of 285 keV for ^{238}U. At this stripping energy the charge state yield is about 42 % when using He-stripping (filled circles in Fig. 4**a**). Below that energy 3+ charge state yields steadily decrease to 36 % at 182 keV. The same trend with energy is observed for the 4+ charge state yields which increase from 6 % (182 keV) to 15 % (281 keV). The 5+ charge state yield was significantly below 1 % for all selected energies and therefore considered negligible. About 20 % of ^{238}U has been found in 2+ charge state at 181 keV but the limited bending power of the HE1 magnet did not allow determination of the 2+ charge state yield at higher energies.

Our results generally fit with published data from other compact AMS systems [7,36,38]. Maximum charge state yields for $^{238}U^{3+}$ of 45 % to 50 % have been reported for stripping energies between 450 keV and 1 MeV [36,38,40]. Existing data obtained with the ETH Tandy system [8] as well as our results consistently confirm the decreasing population of the 3+ charge state at lower energies. Also our yields for the 4+ charge state match reasonably well with literature values indicating a continuously increasing population of this charge state with energy (0.1–1 MeV). Significant differences exist between different facilities regarding the 2+ charge state. Here, results obtained at the ETH Tandy and VEGA facilities are about a factor of two higher than our results and values obtained at SARA (CNA). Possible explanations of this difference may involve ion optical reasons, i.e. problems with the ion beam focusing at lower than nominal energies, or analytical problems, e.g. a misinterpretation of the transient maximum as equilibrium charge state yield. We further note that (except for the 2+) the charge state yields reported from the VEGA facility tend to match with those reported from other facilities at higher energies but tend to fall much steeper at lower energies. This might indicate that a significant fraction of the beam was lost due to improper focusing of the ion beam at low energies.

In this study (MILEA), the charge state yields have been recorded with open slits and with a large FC since we intended to minimize beam losses. For routine measurements smaller FCs are used and apertures are inserted to constrain the beam and to reduce possible background. This results in a lower ^{238}U transmission for routine measurements of $^{236}U/^{238}U$ than presented in this section. The background and sensitivity for routine analyses of $^{236}U/^{238}U$ are described in the following section.

3.2.2. *Transmission and abundance sensitivity*

Measurements presented in this section have been performed with the standard setup for ^{236}U (Fig. 2) using an injection aperture (A3) size of 3 mm (Fig. 1) as this setting provides a good compromise between high background suppression (see next section) and high transmission (red squares in Fig. 5). Due to the existence of molecular background including triply charged UH-molecules [41] measurements of $^{236}U/^{238}U$ have to be carried out at higher than optimal stripper pressure (shaded area in Fig. 5) at a transmission of about 30 %. At He-densities below about 1.4x10^{16} at/cm^2 molecular background is not sufficiently suppressed, which is indicated by both the elevated $^{236}U/^{238}U$ ratio measured for the VKkU sample (blue in Fig. 5) and by exponential increase (worsening) of the AS (purple in Fig. 5). At these low stripper densities the increased AS is not caused by tailing from other U-isotopes (e.g. ^{235}U) but by $^{238}UH^{3+}$ molecules that survive the stripping process [42]. At He stripper gas densities of around 1.7 x10^{16} at/cm^2 molecular background is sufficiently suppressed, which is indicated by the AS reaching a minimum (optimal) value of 5 × 10^{-13}. This setting (shaded area in Fig. 5) is used for routine measurements of $^{236}U/^{238}U$. It provides

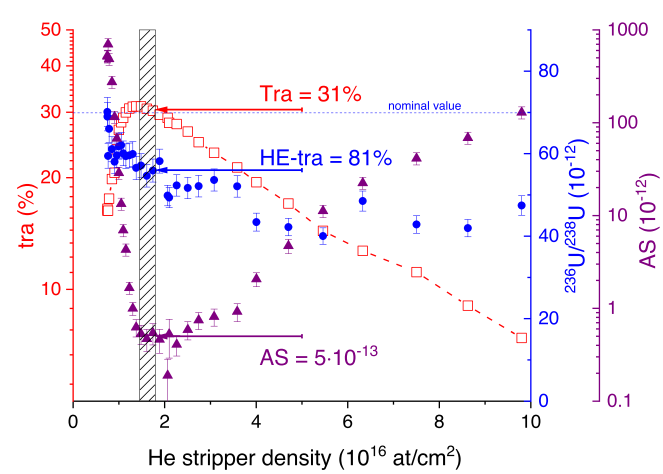

Fig. 5. Abundance sensitivity, transmission and HE-transmission. Abundance sensitivity (purple), transmission (red) and HE-transmission (blue) as a function of He-stripper gas density. The hatched region represents the optimal stripper density for routine analyses of ^{236}U. (For interpretation of the references to colour in this figure legend, the reader is referred to the web version of this article.)

more than 30 % transmission for ^{238}U while the ratio of the VKkU standard is reduced by less than 20 % of its nominal value (blue circles in Fig. 5). At much higher than optimal He stripper gas densities transmission decreases to less than 10 % due to increased scattering losses of the ion beam in the stripper and due to increased energy straggling. At the same time the AS worsens (rising to 10^{-10}) because the increased presence of stripper gas in the acceleration gap increases the probability of charge exchange processes and scattering of background ions such as ^{235}U. Also the $^{236}U/^{238}U$ ratios decrease to about 60 % nominal. This can be explained by increased angular and energy scattering that leads to a larger beam diameter, which in turn leads to increased losses of ^{236}U relative to ^{238}U, because only ^{236}U is confined by additional apertures. We note that even in this unfavorable case the declined AS does not cause an increase of the measured $^{236}U/^{238}U$ ratio of the VKkU sample. An AS of 10^{-10} only causes a theoretical background at the order of 10^{-12}, which is about 2 % of the measured $^{236}U/^{238}U$ ratio of the VKkU sample at high stripper densities.

The VKkU_hc samples used for this and the following background experiments yielded a maximum U^{3+} current of up to 1 μA (range: 0.1–1μA) documenting the high-output capabilities of the MILEA ion source. This further implies that the AS and background measurements could be carried out with good counting statistics as 0.5μA of $^{238}U^{3+}$ current is equivalent to 10^{12} ions/s implying that a ratio of 10^{-12} can be measured at a counting rate of 0.8 counts per second (assuming 80 % HE transmission).

3.2.3. Background scans and aperture settings

Earlier experiments at the compact ETH Zurich TANDY AMS system using a time-of-flight detector showed that the main sources of background for ^{236}U measurements originate from scattered ^{235}U (to a minor extent also from ^{238}U) [9] and from $^{235}UH^{3+}$ molecules [42]. As molecular interferences can be suppressed by choosing an appropriate stripper gas density, ^{235}U (and ^{238}U) remain as most severe sources of background for ^{236}U measurements. Since the setup of the MILEA high-energy side as well as the stripping energies of the actinide ions are comparable with the Tandy system, we expect similar sources of background.

^{235}U is injected into the accelerator together with the $^{236}U^{16}O$, either as a molecule of the same mass (e.g. $^{235}U^{17}O$ or $^{235}U^{1}H^{16}O$) or as a tail from the $^{235}U^{16}O$ beam on the neighboring mass [7]. ^{238}U can also be injected as a molecular isobar ($^{238}U^{14}N$) or as a tail from the intense $^{238}U^{16}O$ beam on amu(254). After breakup of the injected molecules in the stripper $^{235}U^{3+}$ and $^{238}U^{3+}$ can reach the GIC after charge exchange processes in the acceleration gap followed by scattering processes on the HE side [9].

In a first step to investigate the influence of the slit settings on background and transmission, apertures A3, A5, and A6 (positions indicated in Fig. 1) are varied, always starting from the routine setup indicated by the dashed line in Fig. 6, while AS and the HE transmission are recorded (Fig. 6). The variation of the HE-apertures A5 and A6 has a moderate influence on both, AS and HE-transmission. The AS can be reduced by more than a factor of three (from 1×10^{-12} to 0.3×10^{-12}) when closing A5 (A6) from 4.5 to 1.5 mm (5 to 1 mm) while HE-transmission decreases by 25 % (from 80 % to 60 %). The variation of the injection aperture A3 has a significant influence on AS but not on HE transmission. Opening A3 from 3 mm to 3.5 mm increases AS by a factor of eight (from 0.47×10^{-12} to 3.7×10^{-12}), while removing it completely worsens AS by a factor of 74 (to 35×10^{-12}). The setting of A3 appears to be most critical as it prevents the injection of tails from other U-isotopes, and may also reduce hydride (^{235}UH) injection. A more detailed study of the source for this background will be subject of future investigations. We note however, that the worsening of the AS by almost two orders of magnitude still does not have a significant influence on the measured $^{236}U/^{238}U$ ratio of the VKkU-standard (or on any other sample at or above the 10^{-10} level). As argued above, an AS of 10^{-10} will cause a background of 10^{-12} on the $^{236}U/^{238}U$ ratio which is at the order of 2 % of the VKkU standard.

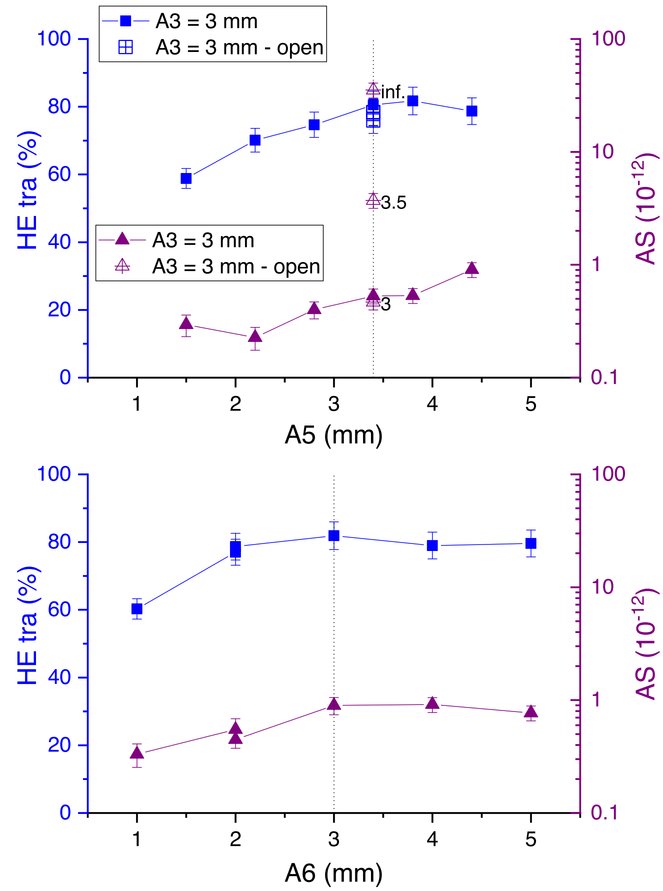

Fig. 6. Abundance sensitivity and HE-transmission for different slit settings. Abundance sensitivity (purple) and HE-transmission (blue) as functions of different aperture openings A3, A5 (upper panel), and A6 (lower panel). The positions of the different apertures are shown in Fig. 1. (For interpretation of the references to colour in this figure legend, the reader is referred to the web version of this article.)

To study in some more detail the sources of background for $^{236}U/^{238}U$ measurements scans of the HE-ESA and the second HE-magnet were carried out at slit settings used for the routine runs (dashed lines in Fig. 6**, and A3** = 3.0 mm). The HE ESA scan shows that after the E/q filter both, ^{235}U and ^{238}U are detected as a possible source of background with ^{235}U representing the higher counting rate (Fig. 7**a**). The position of the ^{235}U peak in the ESA scan corresponds to ^{235}U ions that passed through aperture A5 (Fig. 1) with the same momentum over charge (p/q) ratio as ^{236}U. Different slit widths for A6 (±1, ±1.5, and ± 2 mm) are indicated in Fig. 7 showing that even with small slit settings tails from scattered ^{238}U and ^{235}U ions may enter the next filter (HE2 magnet).

Scanning the HE2 magnet (ESA slits A6 = ±1.5 mm) shows that background from scattered ^{238}U ions has been removed by the second p/q filter (Fig. 7**b**). The only apparent source of background is ^{235}U which appears to enter the HE2 magnet with approximately the same energy over charge (E/q) ratio as ^{236}U. The vertical lines indicate the x-dimension of two possible SiN-window sizes of the GIC for actinide measurements (3x3 mm^2 or 4x4mm^2). Depending on the magnetic field of the HE2 magnet tails of the ^{235}U background might enter the GIC and then be misinterpreted as ^{236}U. A careful tuning of the HE2 magnet is therefore essential to reach good abundance sensitivity and high background suppression because it can significantly reduce the contribution of the ^{235}U tail on ^{236}U. Applying a Gaussian fit to the ^{235}U scan (blue line in Fig. 7) suggests a negligible contribution of ^{235}U to the

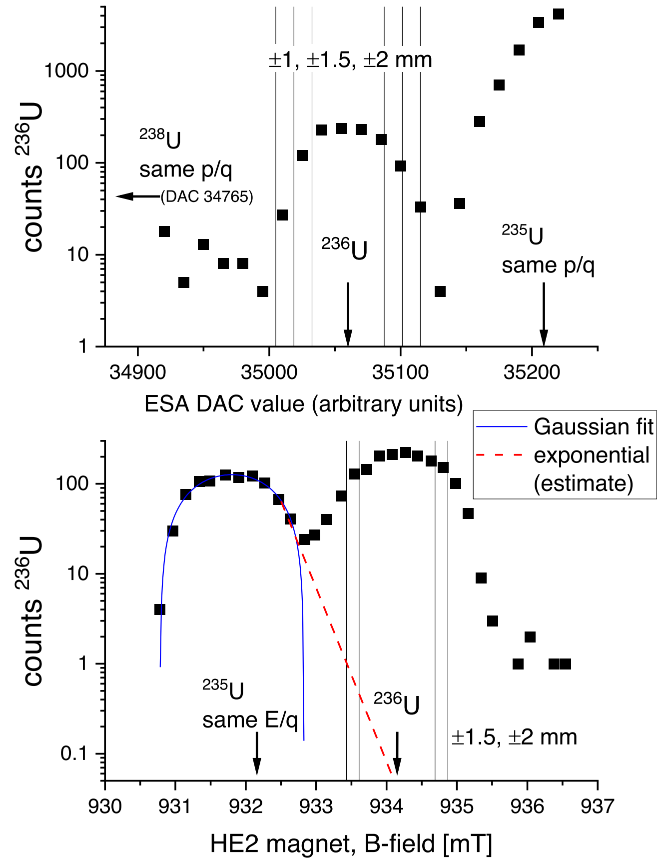

Fig. 7. Background scans ESA, HE2-magnet. Background scans for ^{236}U of the ESA (upper panel) and the second HE-magnet (lower panel). In the ESA scan the calculated positions of ^{235}U and ^{238}U entering with the same momentum over charge ratio as ^{236}U are indicated, while in the HE2-scan the calculated position of ^{235}U entering with the same energy over charge ratio is marked. The vertical lines indicate different openings of A6 (upper panel) and detector window sizes (lower panel), respectively. A Gaussian fit (blue line) is applied to the ^{235}U background peak. The maximum contribution of the ^{235}U tail to ^{236}U after the second HE-magnet is estimated by the simple exponential extrapolation of the ^{235}U tail (red dashed line). (For interpretation of the references to colour in this figure legend, the reader is referred to the web version of this article.)

background on ^{236}U. This is, however, probably an underestimation since the tailing of the background cannot be assumed to be perfectly Gaussian distributed. A more conservative maximum estimate of this background is performed by extrapolating the exponentially decreasing trend of the ^{235}U tail (red dashed line in Fig. 7). The estimated counting rate from this tail is more than 3 orders of magnitude below the maximum counting rate of ^{236}U on the VKkU sample. Considering the nominal ^{236}U/^{238}U ratio of the VKkU of 7×10^{-11} the resulting maximum estimate of background from the ^{235}U tail is 2×10^{-14}. We note that this is (i) a very rough estimation since the shape of the ^{235}U tail is not known, and (ii) that the contribution from this tail to the ^{236}U signal also depends on the tuning of the HE2 magnet and can be reduced by selecting a slightly higher B-field (Fig. 7).

In summary, routine measurements of ^{236}U/^{238}U on the ETH Zurich MILEA system are performed at more than 30 % transmission for ^{238}U while providing an AS of 5×10^{-13} and a HE transmission of more than 80 %. While the low AS indicates a theoretical background at a level of 10^{-15} for ^{236}U/^{238}U the extrapolation of tails from ^{235}U consistently suggest that the background is $<2 \times 10^{-14}$ Together with the high output and efficiency of the MILEA ion source (see next section) such low levels of ^{236}U/^{238}U background will allow assessing the natural levels of ^{236}U/^{238}U in the environment. Lowest ^{236}U/^{238}U ratios were reported from deep Pacific Ocean water samples is in the 10^{-13} range [6]. These results, however were associated with very high (>100 %) uncertainties due to low counting statistics and significant blank corrections. The new MILEA system will allow ^{236}U/^{238}U analyses of such samples with higher efficiency and most probably greater precision.

3.3. Efficiency for U and Pu

To estimate the maximum detection efficiency (EQ (2), section 2.4.4) for U and Pu samples prepared in an oxide matrix, well known amounts of ^{233}U and ^{242}Pu (about 1 pg each) were co-precipitated using different amounts of Fe, then oxidized and mixed with various amounts of Nb powder (Table 1). Two experiments were performed with different ion source settings before (Fig. 8**a and b**) and after modification as described in section 2.2 (Fig. 8**c and d**). In both cases maximum detection efficiencies of almost 1 % are reached for both U (squares) and Pu (circles) which translate into ionization efficiencies for UO^- and PuO^- of more than 3 % (EQ (3)).

Two important differences between the two efficiency tests are noted. First, during the first run UO^- and PuO^- ionization efficiency seemed to be similar with regard to both, temporal evolution (Fig. 8**a**) and absolute values (Fig. 8**b**). The second run with the modified higher output ion source appears to favor UO^- formation over PuO^- formation for all sample matrices (Fig. 8**d**). This effect seems to increase with larger sample size (increasing amounts of Fe and Nb). For example, the sample prepared with 3 mg Fe and 6 mg Nb reached a total detection efficiency of 1 % for ^{233}U but only 0.7 % for ^{242}Pu after 11 h of sputtering time. This effect is currently not understood and requires further investigation. It has however no effect on the routine analysis of actinides since usually only isotopic ratios of the same element are measured. A different (and may be temporarily variable) ionization efficiency of different actinide elements, however, will significantly influence more specialized AMS setups e.g. the analysis of ^{237}Np using a ^{242}Pu spike [43].

The second point is that with the modified (higher output) ion source, maximum detection efficiency of 1 % is reached for ^{233}U after 11 h sputtering time, which is 35 % faster compared to >17 h with the initial setup (Fig. 8**a, c**). The fact that high detection efficiencies now can be reached within more reasonable measurement times implies that larger batches of actinide samples can be analyzed with better precision due to lower uncertainty from counting statistics. For example, with the modified NEC ion source installed at the ETH Zurich Tandy system maximum detection efficiencies at a level of 1–2 ‰ are reached after ca. 3 h sputtering time [7]. With the modified MILEA ion source values of 4.4 ‰ and 3.7 ‰ are reached within the same time for the best performing U and Pu sample, respectively. This implies that twice the amount of counts is acquired for the rare nuclide resulting in a 30 % ($1/\sqrt{2}$) reduced uncertainty due to better counting statistics.

The highest detection efficiency of up to 1.5 % for PuO^- extracted from an oxide matrix has been reported recently using a NEC ion source [36]. The experiment was slightly different from the efficiency tests presented here because the sample containing only 25 fg of Pu was split into two targets and the counts were later combined. The maximum reported detection efficiency was reached after 22 h of combined sputtering time making the highly efficient analysis of larger batches of actinide samples appear unrealistic. Using the average reported counting rate of about 15 cps observed for ^{242}Pu over the first 3 h [36] results in an apparent detection efficiency of 2.6 ‰ for Pu reached after the first 3 h of sputtering time. The apparent detection efficiencies reached after 3 h with the modified MILEA ion source are a factor of 1.4 (Pu) and 1.7 (U) higher. Although the above comparison strongly depends on the ion source settings of each system, our results show that the ETH Zurich MILEA system is ideally suited for the highly efficient and fast analysis of actinides at environmental levels. Although further studies on the different ionization efficiency of actinide elements will be carried out we conclude on the basis of the presented efficiency tests (Fig. 8**d**) that an

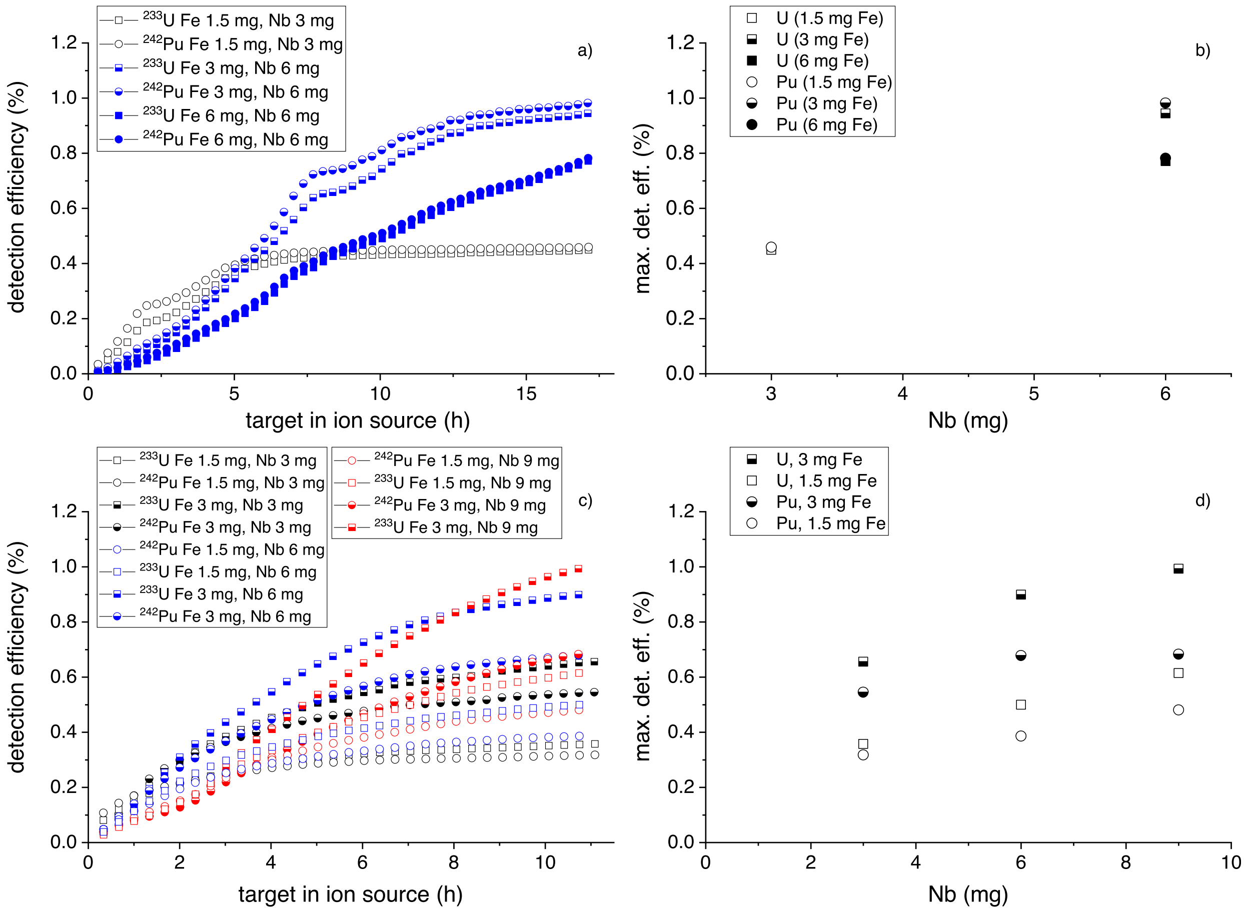

Fig. 8. Efficiency tests. Detection efficiency for U (squares) and Pu (circles) as a function of sputtering time in the ion source. Samples were prepared with a well-known amount of U and Pu (ca. 1 pg), precipitated as hydroxide with different amounts of Fe (1.5 mg: open symbols, 3 mg: half-filled symbols, 6 mg: filled symbols) and mixed with different amounts of Nb powder (3 mg: black, 6 mg: blue, 9 mg: red).Efficiency tests shown in a) and b) were carried out with different ion source settings compared to c) and d) – see main text for details. (For interpretation of the references to colour in this figure legend, the reader is referred to the web version of this article.)

optimal performing oxide matrix for actinide measurement at the ETH Zurich MILEA system contains 3 mg Fe and 6–9 mg of Nb powder.

3.4. Stability and first routine operation

Routine measurements of $^{236}U/^{238}U$ have been carried out with the initial (blue) and the modified (red), high output ion source of MILEA (Fig. 9). The temporal evolution of the normalized $^{x}U/^{238}U$ ratios (with $\times$ = 233, 236, 235) of the ETH Zurich in house Zutri standard [32] is shown over a period of 52 h (red) and 25 h (blue) on the left side of the figure. On the right side, the dependency of the $^{x}U/^{238}U$ ratios on the measured ^{238}U or ^{235}U current is displayed. The lower current output of the standards in the 2019 run is clearly visible. While the standards gave $^{238}U^{3+}$ currents in the range of 0.3–1.6 nA their output increased by more than four times with the modified ion source setup (up to 7 nA). Still, no current dependency of the $^{x}U/^{238}U$ ratios is detected for the high output run (red data).

Although temporal stability was good in both runs, standard deviations of the ratios in 2021 were significantly lower than in the 2019 run due to the higher counting statistics. In this first run in 2021, $^{x}U/^{238}U$ ratios were measured with a standard deviation of 1.6 % ($^{235}U/^{238}U$), 2.0 % ($^{233}U/^{238}U$), and 3.6 % ($^{236}U/^{238}U$). Since these results only reflect one single U-run we consider them preliminary. Future statistics on routine analyses of ^{236}U on MILEA will provide more representative values on long term stability and precision.

In the 2021 run, sea water samples of 1.5–1.9L volume were analyzed for $^{x}U/^{238}U$ ratios with a precision of 3 % or less (results will be published elsewhere). The average $^{238}U^{3+}$ currents of the samples ranged between 1 and 2nA. Assuming 100 % chemical recovery the targets contained not more than 5–7 µg of ^{238}U, which is equivalent to a maximum sensitivity of 400 pA/µg U for sea water samples and five times higher than the maximum sensitivity reported for the ETH Tandy system [44]. The above sensitivity translates into a detection efficiency of 1 ‰ after 3000 s measurement time, which is consistent with the efficiency measurements presented in Fig. 8. Our results thus show that 2 L sea water sampling volume are sufficient to analyze $^{236}U/^{238}U$ ratios of $\geq 10^{-10}$ with 3 % precision or better within less than one hour per sample.

4. Conclusion

Our results demonstrate that the compact, low energy AMS prototype system MILEA allows fast, sensitive, and low background analyses of ^{236}U and Pu-isotopes. It therefore provides a robust and easy to handle analytical tool particularly for analyzing larger batches of small samples as, for example, required for oceanographic surveys. With a background below 2×10^{-14} for $^{236}U/^{238}U$ and a high detection efficiency of up to 1 % for U and Pu, the ETH Zurich MILEA system opens up the field for investigating natural $^{236}U/^{238}U$ in the 10^{-12} range and below while keeping sample sizes/volumes within reasonable limits.

Declaration of Competing Interest

The authors declare the following financial interests/personal

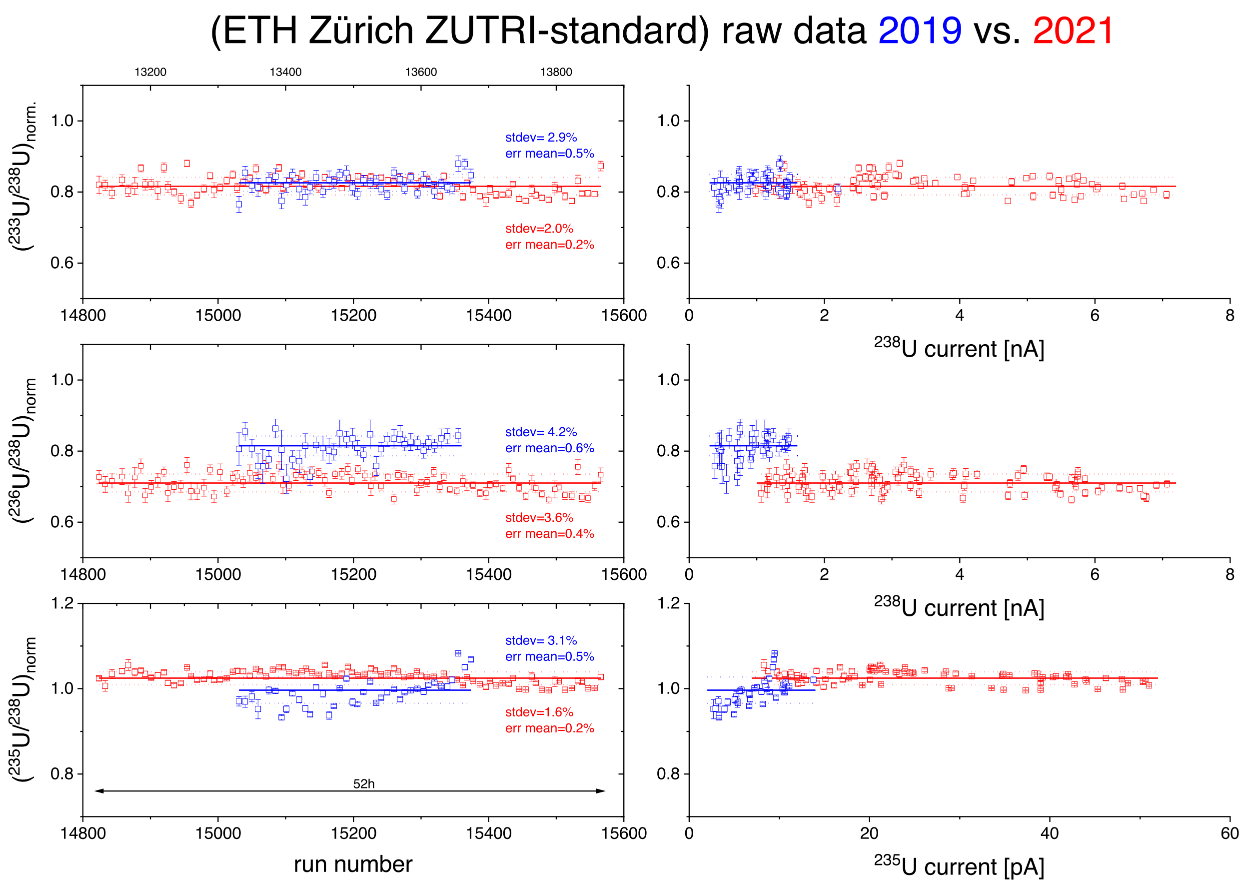

Fig. 9. First routine runs: results from the first routine measurements of u-isotopes carried out in 2019 (blue) and 2021 (red). the measured $^{233}U/^{238}U$, $^{236}U/^{238}U$, and $^{235}U/^{238}U$ ratios of the ETH-Zurich in house standard ZUTRI are shown as a function of time (run number, left side) and as a function of ^{238}U or ^{235}U current (right side). (For interpretation of the references to colour in this figure legend, the reader is referred to the web version of this article.)

relationships which may be considered as potential competing interests:

Marcus Christl reports a relationship with Ionplus AG, Switzerland that includes: equity or stocks. Philip Gautschi reports a relationship with Ionplus AG, Switzerland that includes: equity or stocks. Arnold Milenko Müller reports a relationship with Ionplus AG, Switzerland that includes: board membership, and equity or stocks. Christof Vockenhuber reports a relationship with Ionplus AG, Switzerland that includes: equity or stocks. Hans-Arno Synal reports a relationship with Ionplus AG, Switzerland that includes: board membership and equity or stocks.

The remaining author declare that they have no known competing financial interests or personal relationships that could have appeared to influence the work reported in this paper.

Acknowledgements

The ETH Zurich Laboratory of Ion Beam Physics (LIP) is partially funded by its consortium partners PSI, EMPA, and EAWAG. PG is funded by the Swiss National Science Foundation (grant 200020_197137). We want to thank Kayley Kündig and Gioele Scacco for their dedication in the lab and for preparing numerous U and Pu samples, standards, and efficiency tests.

References

[1] K. Hain, et al., $^{233}U/^{236}U$ signature allows to distinguish environmental emissions of civil nuclear industry from weapons fallout, Nat. Commun. 11 (2020) 1275.

[2] J. Qiao, et al., An unknown source of reactor radionuclides in the Baltic Sea revealed by multi-isotope fingerprints, Nat. Commun. 12 (2021) 823.

[3] M. Christl, J. Lachner, C. Vockenhuber, O. Lechtenfeld, I. Stimac, M.R. van der Loeff, H.-A. Synal, A depth profile of uranium-236 in the Atlantic Ocean, Geochim. Cosmochim. Acta 77 (2012) 98–107.

[4] A. Sakaguchi, et al., Uranium-236 as a new oceanic tracer: a first depth profile in the Japan Sea and comparison with caesium-137, Earth Planet. Sci. Lett. 333–334 (2012) 165.

[5] N. Casacuberta, M. Christl, J. Lachner, M.R. van der Loeff, P. Masqué, H.-A. Synal, A first transect of ^{236}U in the North Atlantic Ocean, Geochim. Cosmochim. Acta 133 (2014) 34–46.

[6] M. Villa-Alfageme, et al., Distribution of ^{236}U in the U.S. GEOTRACES Eastern Pacific Zonal Transect and its use as a water mass tracer, Chem. Geol. 517 (2019) 44.

[7] M. Christl, et al., Status of 236U analyses at ETH Zurich and the distribution of ^{236}U and ^{129}I in the North Sea in 2009, Nucl. Instrum. Methods Phys. Res., Sect. B 361 (2015) 510.

[8] C. Vockenhuber, V. Alfimov, M. Christl, J. Lachner, T. Schulze-König, M. Suter, H.-A. Synal, The potential of He stripping in heavy ion AMS, Nucl. Instrum. Methods Phys. Res., Sect. B 294 (2013) 382–386.

[9] C. Vockenhuber, M. Christl, C. Hofmann, J. Lachner, A.M. Müller, H.-A. Synal, Accelerator mass spectrometry of ^{236}U at low energies, Nucl. Instrum. Methods Phys. Res., Sect. B 269 (24) (2011) 3199–3203.

[10] P. Steier, M. Bichler, L. Keith Fifield, R. Golser, W. Kutschera, A. Priller, F. Quinto, S. Richter, M. Srncik, P. Terrasi, L. Wacker, A. Wallner, G. Wallner, K.M. Wilcken, E. Maria Wild, Natural and anthropogenic ^{236}U in environmental samples, Nucl. Instrum. Methods Phys. Res., Sect. B 266 (10) (2008) 2246–2250.

[11] A. Wallner, et al., ^{60}Fe and ^{244}Pu deposited on Earth constrain the r-process yields of recent nearby supernovae, Science 372 (2021) 742.

[12] C. Tighe, et al., Local and global trace plutonium contributions in fast breeder legacy soils, Nat. Commun. 12 (2021) 1381.

[13] M. López-Lora, et al., ^{236}U, ^{237}Np and $^{239,240}Pu$ as complementary fingerprints of radioactiveeffluents in the western Mediterranean Sea and in the Canada Basin (Arctic Ocean), Sci. Total Environ. 765 (2021), 142741.

[14] Y. Wu, X. Dai, M. Christl, H.-A. Synal, S. Xing, S. Hou, Ultrasensitive analytical method for direct search of primordial ^{244}Pu in Bastnaesite, ACS Earth Space Chem. 5 (6) (2021) 1316–1324.

[15] M. Christl, et al., A novel chronometry technique for dating irradiated uranium fuels using Cm isotopic ratios, J. Radioanal. Nucl. Chem. 322 (2019) 1611.

[16] K. Gückel, et al., Scavenged ^{239}Pu, ^{240}Pu, and ^{241}Am from snowfalls in the atmosphere settling on Mt. Zugspitze in 2014, 2015 and 2016, Sci. Rep. 7 (2017) 11848.
[17] X. Dai, et al., Determination of Atto- to Femtogram levels of americium and curium isotopes in large-volume urine samples by compact accelerator mass spectrometry, Anal. Chem. 88 (2016) 2832.
[18] M. Stocker, et al., A universal and competitive compact AMS facility, Nucl. Instrum. Methods Phys. Res., Sect. B 240 (2005) 483.
[19] L. Wacker, et al., Measurement of actinides on a compact AMS system working at 300 kV, Nucl. Instrum. Methods Phys. Res., Sect. B 240 (2005) 452.
[20] E. Chamizo, et al., Plutonium measurements on the 1 MV AMS system at the Centro Nacional de Aceleradores (CNA), Nucl. Instrum. Methods Phys. Res., Sect. B 266 (2008) 4948.
[21] H.-A. Synal, M. Stocker, M. Suter, A new compact radiocarbon AMS system, Nucl. Instrum. Methods Phys. Res., Sect. B 259 (1) (2007) 7–13.
[22] H.-A. Synal, Developments in accelerator mass spectrometry, Int. J. Mass Spectrom. 349-350 (2013) 192–202.
[23] A.M. Müller, M. Christl, J. Lachner, M. Suter, H.-A. Synal, Competitive ^{10}Be measurements below 1MeV with the upgraded ETH–TANDY AMS facility, Nucl. Instrum. Methods Phys. Res., Sect. B 268 (17-18) (2010) 2801–2807.
[24] M. Suter, et al., Advances in particle identification in AMS at low energies, Nucl. Instrum. Methods Phys. Res., Sect. B 259 (2007) 165.
[25] A.M. Müller, M. Döbeli, M. Suter, H.-A. Synal, Performance of the ETH gas ionization chamber at low energy, Nucl. Instrum. Methods Phys. Res., Sect. B 287 (2012) 94–102.
[26] T. Schulze-König, et al., The dissociation of ^{13}CH and $^{12}CH_2$ molecules in He and N_2 at beam energies of 80–250keV and possible implications for radiocarbon mass spectrometry, Nucl. Instrum. Methods Phys. Res., Sect. B 269 (2011) 34.
[27] S. Maxeiner, et al., Simulation of ion beam scattering in a gas stripper, Nucl. Instrum. Methods Phys. Res., Sect. B 361 (2015) 237.
[28] M. Suter, E. Chamizo, A.M. Müller, H.-A. Synal, The relevance of ion optics for the development of small AMS facilities, Nucl. Instrum. Methods Phys. Res., Sect. B 268 (7-8) (2010) 722–725.
[29] S. Maxeiner, H.-A. Synal, M. Christl, M. Suter, A. Müller, C. Vockenhuber, Proof-of-principle of a compact 300 kV multi-isotope AMS facility, Nucl. Instrum. Methods Phys. Res., Sect. B 439 (2019) 84–89.
[30] S. Maxeiner, Optimizing the designs of next-generation AMS systems, Dissertation, Zurich (2016), https://doi.org/10.3929/ethz-a-010859505.
[31] A.M. Müller, M. Christl, J. Lachner, H.-A. Synal, C. Vockenhuber, C. Zanella, ^{26}Al measurements below 500kV in charge state 2+, Nucl. Instrum. Methods Phys. Res., Sect. B 361 (2015) 257–262.
[32] M. Christl, et al., The ETH Zurich AMS facilities: performance parameters and reference materials, Nucl. Instrum. Methods Phys. Res., Sect. B 294 (2013) 29.
[33] P. Gautschi, et al., MILEA ion source: adapter for Tandy targets. in: H.A. Synal, M. Christl, (Eds.), LIP annual reports, 2019, pp. 151.
[34] J. Heinemeier, et al., The new extended HVE 1MV multi-element AMS system for low background installed at the Aarhus AMS Dating Centre, Nucl. Instrum. Methods Phys. Res., Sect. B 361 (2015) 143.
[35] E. Chamizo, et al., Plutonium measurements on the 1MV AMS system at the Centro Nacional de Aceleradores (CNA), Nucl. Instrum. Methods Phys. Res., Sect. B 266 (2008) 4948.
[36] M.A.C. Hotchkis, et al., Actinides AMS on the VEGA accelerator, Nucl. Instrum. Methods Phys. Res., Sect. B 438 (2019) 70.
[37] P. Hvelplund, Energy loss and straggling of 100–500 keV atoms with $2 \leq Z_1 \leq 12$ In Various Gases, Munksgaard, København, 1971.
[38] E. Chamizo, M. López-Lora, Accelerator mass spectrometry of ^{236}U with He stripping at the Centro Nacional de Aceleradores, Nucl. Instrum. Methods Phys. Res., Sect. B 438 (2019) 198.
[39] J.F. Ziegler, M.D. Ziegler, J.P. Biersack, SRIM – The stopping and range of ions in matter (2010), Nucl. Instrum. Methods Phys. Res., Sect. B 268 (11-12) (2010) 1818–1823.
[40] S.R. Winkler, et al., He stripping for AMS of ^{236}U and other actinides using a 3MV tandem accelerator, Nucl. Instrum. Methods Phys. Res., Sect. B 361 (2015) 458.
[41] J. Lachner, et al., Existence of triply charged actinide-hydride molecules, Phys. Rev. A 85 (2012), 022717.
[42] J. Lachner, et al., Detection of UH^{3+} and ThH^{3+} molecules and ^{236}U background studies with low-energy AMS, Nucl. Instrum. Methods Phys. Res., Sect. B 294 (2013) 364.
[43] M. López-Lora, E. Chamizo, Accelerator Mass Spectrometry of 237Np, 239Pu and 240Pu for environmental studies at the Centro Nacional de Aceleradores, Nucl. Instrum. Methods Phys. Res., Sect. B 455 (2019) 39.
[44] M. Christl, et al., ^{236}U/^{238}U measurements on the Tandy. in: H.A. Synal, M. Christl, (Eds.), LIP annual reports, Zurich, 2019, pp. 151.